ACS OMEGA

http://pubs.acs.org/journal/acsodf

Article

Plasmonic Nanostructures-Decorated ZIF-8-Derived Nanoporous Carbon for Surface-Enhanced Raman Scattering

Guan-Ye Liao, Mei-Chin Lien, Sirimuvva Tadepalli, and Keng-Ku Liu*

Cite This: *ACS Omega* 2022, 7, 36427−36433

Read Online

ACCESS | Metrics & More | Article Recommendations | Supporting Information

ABSTRACT: Surface-enhanced Raman scattering (SERS) is considered to be a highly sensitive platform for chemical and biological sensing. Recently, owing to their high porosity and large surface area, metal−organic frameworks (MOFs) have attracted considerable attention in sensing applications. Porous carbon nanostructures are promising SERS substrates due to their strong broadband charge-transfer resonance and reproducible fabrication. Furthermore, an extraordinarily large enhancement of the electromagnetic field enables plasmonic nanomaterials to be ideal SERS substrates. Here, we demonstrate the porous Au@Ag nanostructure-decorated MOF-derived nanoporous carbon (NPC) for highly efficient SERS sensing. Specifically, this plasmonic nanomaterial−NPC composite offers high Raman signal enhancement with the ability to detect the model Raman reporter 2-naphthalenethiol (2-NT) at picomolar concentration levels.

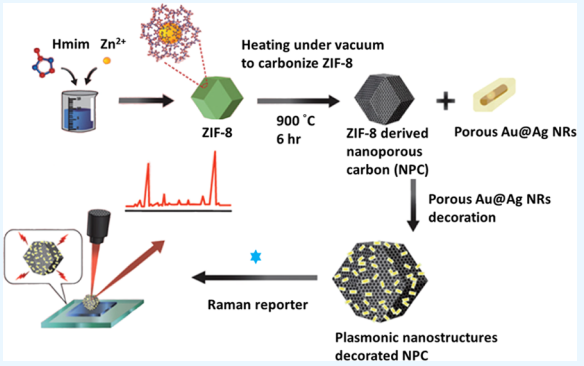

INTRODUCTION

Sensitive and rapid detection of analytes is of great importance in the fields ranging from clinical diagnosis, biomedical research, analytical chemistry, and food safety to environmental sciences.[1−3] Surface-enhanced Raman scattering (SERS) is considered to be a highly sensitive and promising technique for chemical and biological sensing.[4−7] The capability to identify the analyte from characteristic fingerprints enables this technique to be utilized for trace detection of analytes.[8,9] In the past few decades, extensive research efforts have been dedicated to the design and formation of the SERS substrates with both large SERS enhancement and high reproducibility.[1,10−12]

Noble metal nanomaterials have been employed in a variety of biomedical applications, including imaging, drug delivery, and sensing.[13−18] Many of these applications rely heavily on their unique optical properties resulting from localized surface plasmon resonance (LSPR).[13−15,17] Phenomenal progress in the synthesis of size- and shape-controlled plasmonic nanostructures with tunable LSPR wavelength in the visible range to parts of the near-infrared range has led to these nanostructures as powerful nanomaterials for analytical platforms.[17,19,20] The strong electric field on the surface of plasmonic nanostructures, as well as the hotspots formed between the nanostructures, suggests that the plasmonic nanostructures are ideal for SERS-based sensing applications.[21,22] Metal−organic frameworks (MOFs), consisting of metal ions or clusters linked by organic ligands, are a relatively new class of hybrid organic−inorganic supramolecular materials and have attracted great research attention due to their tunable porosity and large surface area.[23−25] These attractive properties, owing to their porous nature, render novel MOF materials for catalysts, gas storage, drug delivery, and chemical sensing.[26−33] Recently, porous carbon nanostructures have been demonstrated as an effective substrate for highly sensitive and biocompatible SERS sensing.[34] The large chemical enhancement due to the strong broadband charge-transfer resonance and reproducible fabrication process makes porous carbon nanostructures promising SERS substrates. Among the methods for the preparation of porous carbon nanomaterials, the direct carbonization of porous MOFs has been considered to be a rapid and effective way.[35] To the best of our knowledge, there have been rare reports on the employment of plasmonic nanomaterials/MOF-derived porous carbon composites for sensing application.

In this work, we report the plasmonic nanostructure decoration on the surface of MOF-derived nanoporous carbon (NPC) for SERS detection. Taking advantage of the porous nature of MOFs as well as the uniformity and strong charge-transfer resonance of porous carbon nanostructures, we demonstrate that the plasmonic nanostructure decoration on the surface of MOF-derived NPC provides not only high signal

Received: July 4, 2022
Accepted: September 23, 2022
Published: October 4, 2022

https://doi.org/10.1021/acsomega.2c04183
ACS Omega 2022, 7, 36427−36433

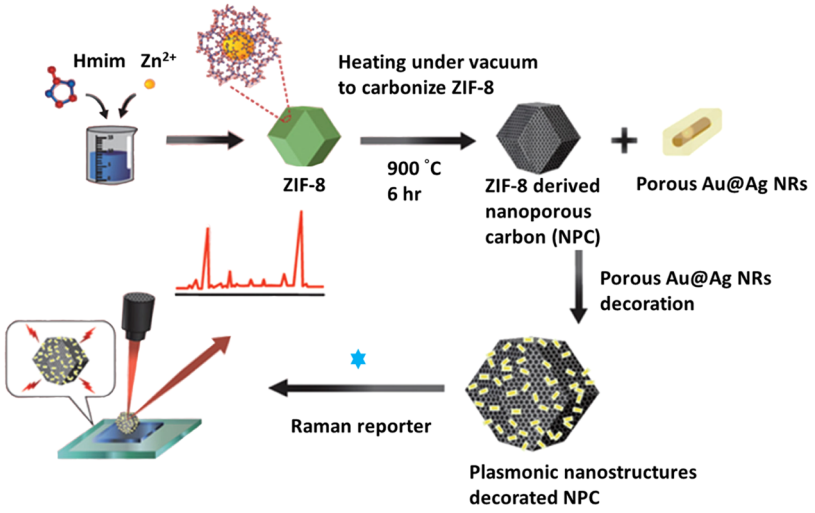

Figure 1. Schematic illustration depicting the fabrication of plasmonic nanomaterial-decorated ZIF-8-derived nanoporous carbon for SERS detection.

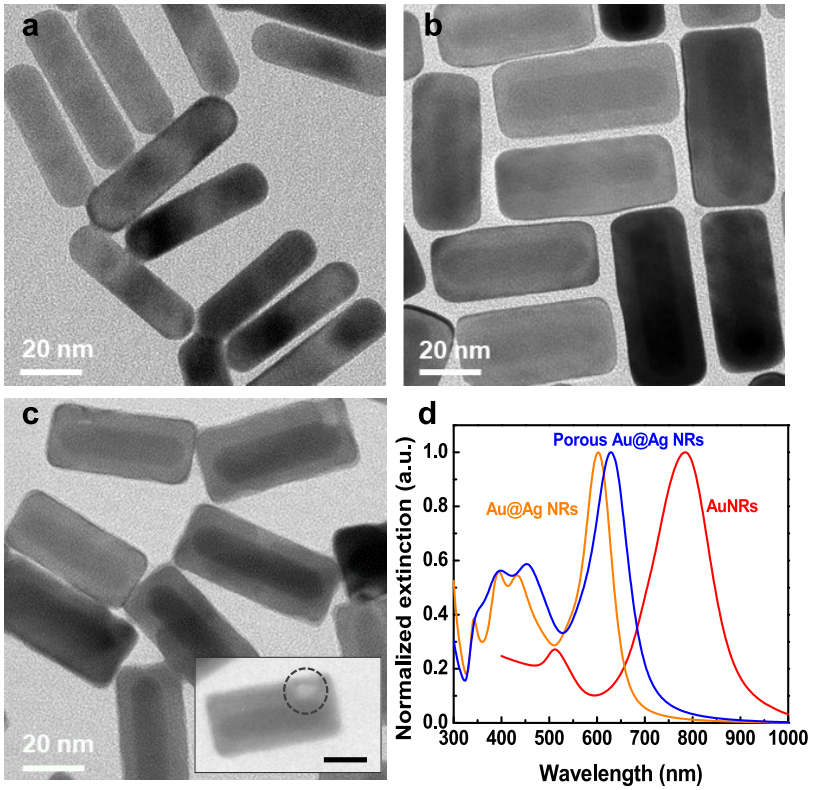

Figure 2. TEM images of (a) AuNRs, (b) Au@Ag NRs, and (c) porous Au@Ag NRs. Inset in panel (c) shows a porous structure with a scale bar of 20 nm. (d) UV−vis−NIR spectra of AuNRs, Au@Ag NRs, and porous Au@Ag NRs.

enhancement but also high reproducibility in the SERS spectrum.

RESULTS AND DISCUSSION

Figure 1 illustrates the fabrication of plasmonic nanomaterial-decorated MOF-derived NPC for SERS detection. Porous core−shell nanostructures consisting of plasmonic Au nano-octahedron as core and porous Au nanocage as shell have recently been demonstrated with higher SERS enhancement due to the electromagnetic hotspots within the nanostructures.[36] Galvanic replacement, which involves the oxidation of one metal with lower reduction potential by the ions of another metal with higher reduction potential, is a versatile method for the synthesis of bimetallic (Au, Ag, Pt, or Pd) and porous core−shell nanostructures with morphology-controllable and wavelength-tunable properties.[37−40] Herein, a two-step process was used for the synthesis of porous core−shell nanostructures. In the first step, a seed-mediated method was employed to synthesize gold nanorods (AuNRs).[41,42] The length and diameter of AuNRs were measured to be around 54 ± 4.2 and 15 ± 1.4 nm, respectively, using transmission electron microscopy (TEM) images (Figure 2a). Silver-coated gold nanorods (Au@Ag NRs) were synthesized using a

https://doi.org/10.1021/acsomega.2c04183
ACS Omega 2022, 7, 36427−36433

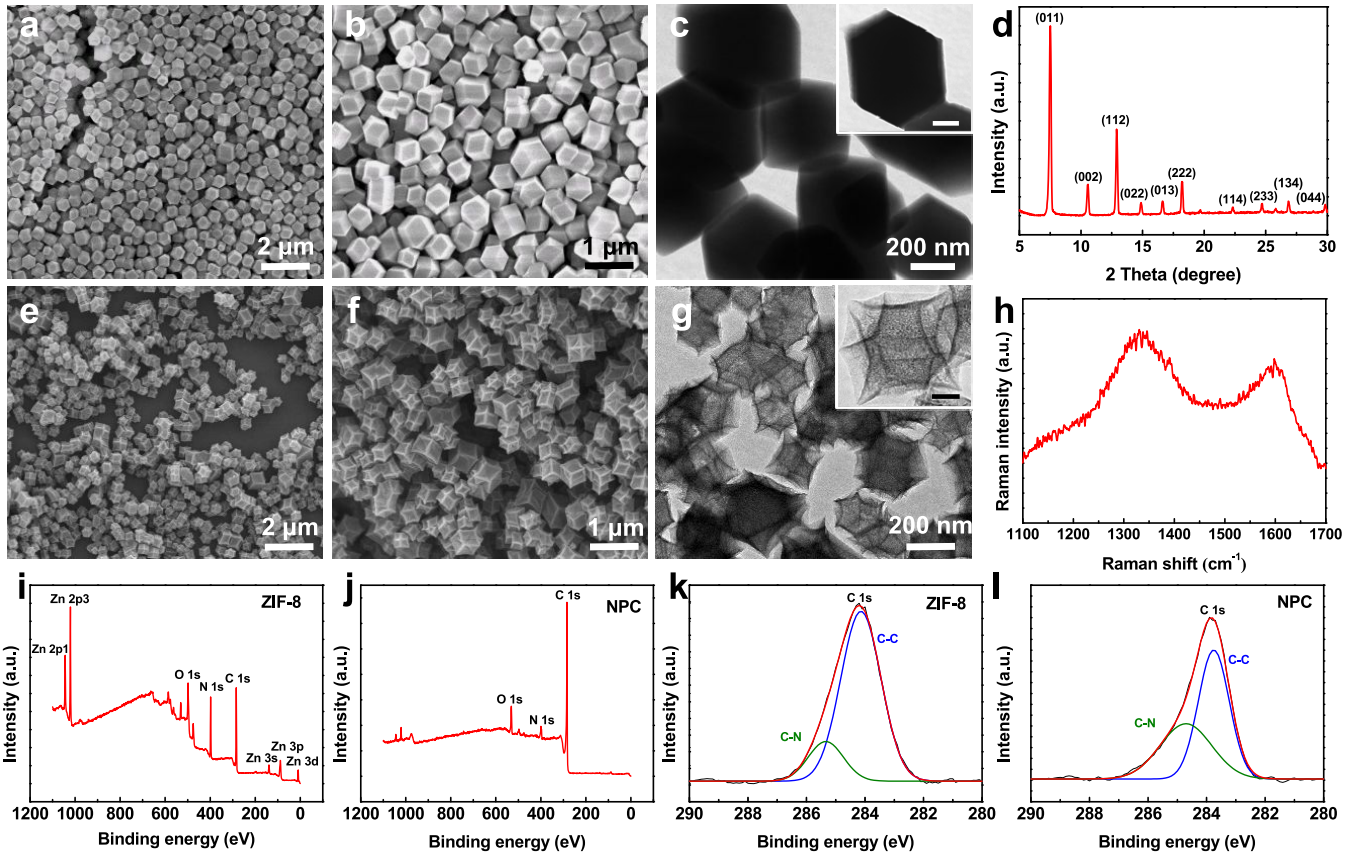

Figure 3. SEM images of ZIF-8 with relatively (a) low and (b) high magnification. (c) TEM image of ZIF-8. Inset shows the representative TEM image of ZIF-8 with a scale bar of 200 nm. (d) XRD pattern of ZIF-8. SEM images of the ZIF-8-derived nanoporous carbon (NPC) with relatively (e) low and (f) high magnification. (g) TEM image of the NPC. Inset shows the representative TEM image of NPC with a scale bar of 100 nm. (h) Raman spectrum of the NPC. XPS survey scans of (i) ZIF-8 and (j) NPC. XPS spectra of (k) ZIF-8 and (l) NPC show the binding energy for carbon (C 1s).

recently reported method with slight modification.[10] Basically, the AuNRs served as the cores in the growth solution consisting of silver nitrate as the Ag precursor, hexadecyltrimethylammonium chloride (CTAC) as the surfactant, and ascorbic acid as the reducing agent. From the TEM image, the length and width of the Au@Ag NRs were measured to be around 57 ± 5.1 and 25 ± 2.2 nm, respectively (Figure 2b). As mentioned above, the galvanic replacement reaction is a facile method for the preparation of hollow and porous bimetallic nanostructures with tunable LSPR wavelength. To achieve a high SERS signal, the galvanic replacement reaction is employed to tailor the LSPR wavelength of the bimetallic nanostructures. The titration of $HAuCl_4$ aqueous solution into the Au@Ag NR solution was controlled to obtain an LSPR band of hollow and porous core−shell nanostructures to be maximally overlapped with the laser excitation of a Raman spectrometer. Adding the aqueous solution of $HAuCl_4$ into the Au@Ag NRs, the progressive red shift in the LSPR wavelength was observed and the hollow and porous Au@Ag nanostructures were formed (Figure S1). The length and width of the porous Au@Ag NRs were measured to be around 58 ± 4.2 and 26 ± 2.8 nm, respectively, and the porous structure can be observed from the TEM images (Figure 2c). The UV−vis−NIR spectra of the AuNRs, Au@Ag NRs, and porous Au@Ag NRs were collected in the solution and are shown in Figure 2d. The UV−vis−NIR spectrum reveals that the AuNRs exhibited transverse and longitudinal plasmon resonance bands at 512 and 785 nm, respectively. For Au@Ag NRs, the LSPR peak at the wavelength around 605 nm is ascribed to the longitudinal dipolar plasmon mode.[43,44] The main peak of the porous Au@Ag NRs was measured to be around 630 nm in the UV−vis−NIR spectrum. The porous structure of the Au@Ag NRs and histogram of the size distribution of the AuNRs, Au@Ag NRs, and porous Au@Ag NRs as measured from TEM images are shown in Figure S2 and S3, respectively.

We then turn our attention to the fabrication and characterization of MOF and NPC. The typical MOFs, zeolitic imidazolate framework-8 (ZIF-8), were synthesized by the mixture of 2-methylimidazole and zinc nitrate hexahydrate in methanol at room temperature (the detailed procedure is provided in the Experimental Section). From the SEM images of the ZIF-8 crystals synthesized with various molar ratios of 2-methylimidazole and zinc nitrate hexahydrate, the size of the crystal was found to be decreased as the ratio of 2-methylimidazole and zinc nitrate hexahydrate increased (Figure S4). 2-Methylimidazole and zinc nitrate hexahydrate at a molar ratio of 4:1 were selected due to the relatively large size of the particle (Figure 3a,b). The size of the ZIF-8 nanostructures was measured to be around 0.5−1 μm from TEM (Figure 3c). X-ray diffraction (XRD) analysis was performed to confirm the crystal structure of ZIF-8 nanostructures. The XRD peak positions as well as the thermogravimetric analysis (TGA) and differential scanning calorimetry (DSC) curves of the as-synthesized ZIF-8 crystals

https://doi.org/10.1021/acsomega.2c04183
ACS Omega 2022, 7, 36427−36433

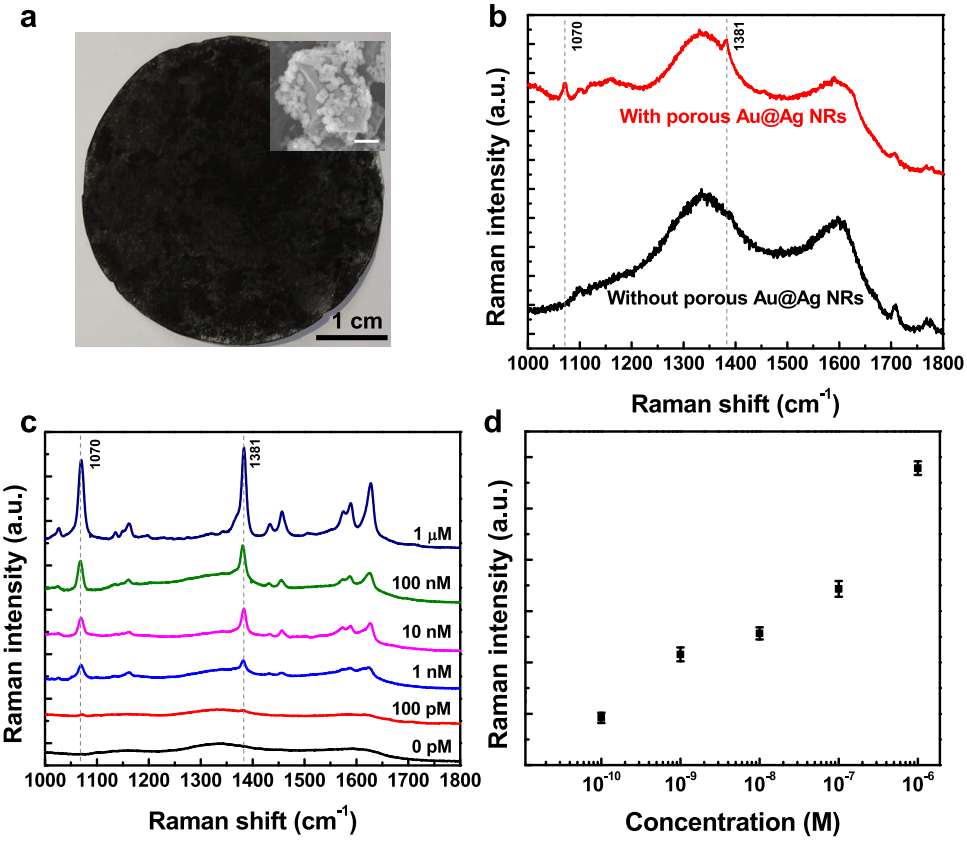

Figure 4. (a) Optical image of the porous Au@Ag NR-coated NPC on the paper substrate. Inset shows the SEM image of the porous Au@Ag NR-coated NPC with a scale bar of 200 nm. (b) Raman spectra of 2-NT (100 pM) on NPC with and without porous Au@Ag NR decoration. (c) Raman spectra of 2-NT at various concentrations on the porous Au@Ag NR-decorated NPC. (d) Plot showing the Raman intensity of the 1381 cm^{-1} Raman band at various concentrations of 2-NT.

were in agreement with the typical structure of ZIF-8 (Figures 3d and S5).[45−47] For the preparation of NPC nanostructures, direct carbonization of ZIF-8 crystals was employed according to a previously reported method with slight modification.[47] Briefly, the ZIF-8 crystals were heated without any additional carbon precursor under an argon atmosphere at 900 °C for 6 h (Figure 3e,3f). From the TEM images, it reveals that the size of the NPC nanostructures is in the range of 0.3−0.6 μm, which is slightly shrank owing to the cleavage of the organic ligands in the carbonization process (Figure 3g). Raman spectrum of the NPC nanostructures revealed the characteristic G-band at the wavenumber of around 1580−1600 cm^{-1} and D-band at the wavenumber of around ∼1330−1350 cm^{-1}, which correspond to the graphitic structure and the disordered carbon structures, respectively (Figure 3h). The surface area of the ZIF-8 nanostructures was calculated to be around 1430 m^2/g by the Brunauer−Emmett−Teller (BET) method, which was close to the reported value (Table S2).[48,49] Compared with the original ZIF-8 nanostructures, the surface area of the NPC nanostructures was reduced to be around 1099 m^2/g, and this was probably the result of the dimensional shrinkage in the carbonization process.[50] X-ray photoelectron spectroscopy (XPS) was employed to investigate the chemical composition of the ZIF-8 and NPC nanostructures (Figure 3i−l and Figure S6). The XPS spectrum of ZIF-8 reveals the presence of C, N, O, and Zn elements (Figure 3i). While in the XPS spectrum of NPC, only the high-intensity peak of C and the relatively weak peaks of N and O are present, indicating that the content of Zn is low due to the evaporation during the carbonization process (Figure 3j). The 1s spectra of carbon can be deconvoluted into two peaks corresponding to the C−C bond with a binding energy of around 284.1 eV and the C−N bond with a binding energy of around 285.4 eV (Figure 3k,l).[51] The elemental mapping results reveal that the content of Zn is rich in ZIF-8 and less in NPC, while the content of C is rich in NPC (Figure S7). The FTIR spectrum of the ZIF-8 crystals shows the main bands at 3135, 1576, 1418, 1328, and 1146 cm^{-1}, which are in consistent with the previously reported literature (Figure S8).[52] The FTIR band at 3135 cm^{-1} was associated with the aromatic C−H stretching vibration, while the band at 1576 cm^{-1} corresponded to the C═N stretch vibration. The bands at 1300−1460 and 1146 cm^{-1} were assigned for the ring stretching and the aromatic C−N stretching modes, respectively. In the XRD spectrum of NPC nanostructures, a broad diffraction band at 25° can be observed, which is assigned to the (002) diffraction of graphitic carbon (Figure S9).[47]

Paper has been demonstrated to be an attractive substrate for flexible biochips owing to their unique properties, such as flexibility, high specific surface area, and abundance.[1,53] Hence, paper has been employed as the flexible substrate in this study. We first decorated plasmonic nanostructures on NPC, which shows the uniform adsorption of porous Au@Ag NRs on NPC (Figures S10 and S11). A simple filtration method was employed to realize the paper-based flexible SERS substrates, which showed that the surface of NPC was coated with a large number of porous Au@Ag NRs (Figure 4a). The SERS substrates demonstrate the robusticity after exposure to

https://doi.org/10.1021/acsomega.2c04183
ACS Omega 2022, 7, 36427−36433

ethanol various times (Figure S12). To investigate the SERS activity, we first exposed the NPC paper with and without plasmonic nanostructure decoration to the same concentration of the Raman reporter, 2-naphthalenethiol (2-NT). The Raman spectra were collected using a 632.8 nm laser as an excitation source. From the Raman spectrum of 2-NT-exposed plasmonic nanostructure-decorated NPC paper, it clearly revealed that the Raman bands at 1070 and 1381 cm^{-1} correspond to the C−H bending and ring stretch vibrations of 2-NT, respectively (Figure 4b).[36] The strong Raman signals of 2-NT were arising from the hotspots of the porous Au@Ag NRs and the charge transfer between the molecule and NPC. While in the Raman spectrum of 2-NT-exposed NPC paper without plasmonic nanostructure decoration, no distinguishable Raman bands of 2-NT can be observed. These results clearly indicate that the SERS substrates prepared by the adsorption of porous Au@Ag NRs on NPC can lead to the generation of high intensity of Raman signal. SERS spectra obtained from the plasmonic nanostructure-decorated NPC paper after exposure to different concentrations of 2-NT are shown in Figure 4c. The most prominent Raman bands of 2-NT appeared at 1070, 1381, and 1627 cm^{-1}, and the Raman band at 1381 cm^{-1} was used to determine the trace detection ability of the plasmonic nanostructure-decorated NPC paper. From the plot of the relationship between the concentration of 2-NT and the Raman intensity, it clearly revealed that the SERS intensity increases with the increase in the concentration of the analyte (Figure 4d). The SERS signals of 2-NT at the concentration of 100 pM can still be observed, which indicates that the porous Au@Ag NR-decorated NPC papers are promising SERS substrates for trace detection.

CONCLUSIONS

In summary, we have demonstrated the fabrication of porous Au@Ag nanostructures and MOF-derived nanoporous carbon for SERS detection. By incorporating the porous Au@Ag NRs into the nanoporous carbon, the SERS signals can be significantly improved. This sensing platform is promising for the applications in chemical and biological sensing applications.

EXPERIMENTAL SECTION

Materials and Chemicals. Gold chloride trihydrate ($HAuCl_4 \cdot 3H_2O$), hexadecyltrimethylammonium bromide (CTAB), sodium borohydride ($NaBH_4$), silver nitrate ($AgNO_3$), ascorbic acid, zinc nitrate hexahydrate (reagent grade, 98%), 2-methylimidazole, and 2-naphthalenethiol (2-NT) were purchased from Sigma-Aldrich. Hexadecyltrimethylammonium chloride (CTAC) was purchased from Tokyo Chemical Industry (TCI). All chemicals were used as received without further purification.

Synthesis of Au Nanorods. Au nanorods were synthesized using the seed-mediated method.[41,42] A seed solution was synthesized by adding 0.6 mL of an ice-cold $NaBH_4$ (10 mM) solution into the solution containing 0.25 mL of $HAuCl_4$ (10 mM) and 9.75 mL of CTAB (0.1 M) under vigorous stirring at room temperature. The color of the seed solution changed from yellow to brown. Growth solution was prepared by mixing 5 mL of $HAuCl_4$ (10 mM), 95 mL of CTAB (0.1 M), 1 mL of $AgNO_3$ (10 mM), and 0.55 mL of ascorbic acid (0.1 M) consecutively. The solution was homogenized by gentle shaking. To the colorless solution, 0.12 mL of freshly prepared seed solution was added and kept undisturbed in the dark for 14 h. Prior to use, the AuNR solution was centrifuged twice at 8000 rpm for 10 min to remove excess CTAB and redispersed in nanopure water.

Synthesis of Au@Ag NRs. Four milliliters of AuNRs was centrifuged twice and 8 mL of CTAC (20 mM) were mixed at 60 °C under stirring for 20 min. Then, 1.6 mL of $AgNO_3$ (2 mM), 2 mL of CTAC (20 mM), and 0.8 mL of ascorbic acid (0.1 M) were added under stirring at 60 °C for 4 h. The Au@Ag NR solution was centrifuged at 8000 rpm for 10 min and redispersed in 50 mM CTAC solution.

Synthesis of Porous Au@Ag NRs. Porous Au@Ag NRs were synthesized by transforming the Ag shell of Au@Ag NRs into the porous shell of Au via the galvanic replacement reaction. The as-synthesized Au@Ag NRs were centrifuged and redispersed in the CTAC solution (20 mM). $HAuCl_4$ aqueous solution (0.5 mM) was injected into the Au@Ag NR solution at a rate of 0.5 mL/min under magnetic stirring.

Synthesis of ZIF-8. ZIF-8 was synthesized according to a previous report with slight modification.[54] Briefly, 10 mL of zinc nitrate hexahydrate (0.2 M in methanol) and 10 mL of 2-methylimidazole (0.8 M in methanol) were mixed with gently stirring at room temperature for 10 min and kept undisturbed for 14 h. The ZIF-8 nanocrystals were washed with methanol through centrifugation and dried at 80 °C for further use.

Synthesis of ZIF-8-Derived Nanoporous Carbon. ZIF-8-derived nanoporous carbon was prepared by carbonization of the ZIF-8 nanocrystals. Basically, the ZIF-8 nanocrystals were heated from room temperature to 900 °C at a rate of 5 °C/min and kept at 900 °C for 6 h under an argon flow.

Spectroscopy Measurements. SERS spectra measurements were performed by adding 2-NT (in ethanol) to the plasmonic nanomaterial-decorated NPC. SERS spectra were collected using a confocal Raman spectrometer (LABRAM HR 800 UV, Horiba Jobin Yvon, Japan). Spectra were collected using the 632.8 nm laser, which was focused on the sample using a 50× objective. At least three spectra were collected from different spots across each sample.

Fabrication of Porous Au@Ag NR-Decorated NPC on Paper Substrates. Porous Au@Ag NR-decorated NPC on paper substrates was fabricated via a vacuum-assisted filtration method. Briefly, 3 mL of NPC (in water, around 67 mg/mL) was filtered, followed by 12 mL of porous Au@Ag NRs (extinction ∼2) on paper substrates.

Characterization. UV−vis extinction spectra were collected using a Shimadzu UV-1900 UV−vis spectrophotometer. Scanning electron microscopy (SEM) images were obtained using a JEOL JSM-7000F field-emission SEM at an accelerating voltage of 10 kV. Transmission electron microscopy (TEM) images were collected using a JEOL JEM-2100 field-emission microscope. ICP-MS measurements were performed using an Agilent 7500ce spectrometer. XPS spectra were obtained using a ULVAC-PHI high-resolution electron spectrometer. The X-ray diffraction (XRD) measurements of the samples were collected using a Rigaku TTRAX III X-ray powder diffractometer. Fourier transform infrared spectroscopy (FTIR) measurements were performed using a Bruker Vertex 80v spectrometer.

ASSOCIATED CONTENT

Supporting Information

The Supporting Information is available free of charge at https://pubs.acs.org/doi/10.1021/acsomega.2c04183.

https://doi.org/10.1021/acsomega.2c04183
ACS Omega 2022, 7, 36427−36433

Representative SEM images, UV−vis−NIR spectra of the Au@Ag NRs, porous Au@Ag NRs and TEM image of the porous Au@Ag NRs; size distribution of the AuNRs, Au@Ag NRs, and porous Au@Ag NRs; ICP-MS analysis; SEM images, TGA, and DSC of ZIF-8; and BET, XPS, elemental mapping, and FTIR of ZIF-8 and NPC (PDF)

AUTHOR INFORMATION

Corresponding Author

Keng-Ku Liu − *Department of Biomedical Engineering and Environmental Sciences, National Tsing Hua University, Hsinchu 300044, Taiwan;* orcid.org/0000-0002-1427-3494; Email: kkliu@mx.nthu.edu.tw

Authors

Guan-Ye Liao − *Department of Biomedical Engineering and Environmental Sciences, National Tsing Hua University, Hsinchu 300044, Taiwan*

Mei-Chin Lien − *Department of Biomedical Engineering and Environmental Sciences, National Tsing Hua University, Hsinchu 300044, Taiwan*

Sirimuvva Tadepalli − *Microbiology & Immunology Department and Immunology Program, Stanford University School of Medicine, Stanford, California 94305, United States;* orcid.org/0000-0001-9658-9988

Complete contact information is available at: https://pubs.acs.org/10.1021/acsomega.2c04183

Author Contributions

K.K.L. and S.T. conceived the project and designed the experiments. G.Y.L. and M.C.L. synthesized the plasmonic nanostructures, MOF, and NPC. G.Y.L. performed the SEM experiments and SERS measurements. K.K.L., G.Y.L., S.T., and M.C.L. wrote and revised the paper. All authors reviewed and commented on the manuscript.

Notes

The authors declare no competing financial interest.

ACKNOWLEDGMENTS

The authors acknowledge the support from the Ministry of Science and Technology (MOST-110-2222-E-007-001-MY3), the Instrumentation Center (MOST 111-2731-M-007-001) and the Department of Biomedical Engineering and Environmental Sciences at National Tsing Hua University for support. They would like to thank Prof. Ruey-An Doong at the National Tsing Hua University for constructive discussions.

REFERENCES

(1) Lee, C. H.; Tian, L.; Singamaneni, S. Paper-Based SERS Swab for Rapid Trace Detection on Real-World Surfaces. *ACS Appl. Mater. Interfaces* **2010**, *2*, 3429−3435.

(2) Lee, C. H.; Hankus, M. E.; Tian, L.; Pellegrino, P. M.; Singamaneni, S. Highly Sensitive Surface Enhanced Raman Scattering Substrates Based on Filter Paper Loaded with Plasmonic Nanostructures. *Anal. Chem.* **2011**, *83*, 8953−8958.

(3) Tian, L.; Liu, K.-K.; Morrissey, J. J.; Gandra, N.; Kharasch, E. D.; Singamaneni, S. Gold nanocages with built-in artificial antibodies for label-free plasmonic biosensing. *J. Mater. Chem. B* **2014**, *2*, 167−170.

(4) Ko, H.; Singamaneni, S.; Tsukruk, V. V. Nanostructured Surfaces and Assemblies as SERS Media. *Small* **2008**, *4*, 1576−1599.

(5) Er, E.; Sánchez-Iglesias, A.; Silvestri, A.; Arnaiz, B.; Liz-Marzán, L. M.; Prato, M.; Criado, A. Metal Nanoparticles/MoS2 Surface-Enhanced Raman Scattering-Based Sandwich Immunoassay for α-Fetoprotein Detection. *ACS Appl. Mater. Interfaces* **2021**, *13*, 8823−8831.

(6) Kamińska, A.; Winkler, K.; Kowalska, A.; Witkowska, E.; Szymborski, T.; Janeczek, A.; Waluk, J. SERS-based Immunoassay in a Microfluidic System for the Multiplexed Recognition of Interleukins from Blood Plasma: Towards Picogram Detection. *Sci. Rep.* **2017**, *7*, No. 10656.

(7) Golightly, R. S.; Doering, W. E.; Natan, M. J. Surface-Enhanced Raman Spectroscopy and Homeland Security: A Perfect Match? *ACS Nano* **2009**, *3*, 2859−2869.

(8) Chen, J.; Liu, G.; Zhu, Y.-z.; Su, M.; Yin, P.; Wu, X.-j.; Lu, Q.; Tan, C.; Zhao, M.; Liu, Z.; Yang, W.; Li, H.; Nam, G.-H.; Zhang, L.; Chen, Z.; Huang, X.; Radjenovic, P. M.; Huang, W.; Tian, Z.-q.; Li, J.-f.; Zhang, H. Ag@MoS2 Core−Shell Heterostructure as SERS Platform to Reveal the Hydrogen Evolution Active Sites of Single-Layer MoS2. *J. Am. Chem. Soc.* **2020**, *142*, 7161−7167.

(9) Cialla-May, D.; Zheng, X. S.; Weber, K.; Popp, J. Recent progress in surface-enhanced Raman spectroscopy for biological and biomedical applications: from cells to clinics. *Chem. Soc. Rev.* **2017**, *46*, 3945−3961.

(10) Liu, K.-K.; Tadepalli, S.; Tian, L.; Singamaneni, S. Size-Dependent Surface Enhanced Raman Scattering Activity of Plasmonic Nanorattles. *Chem. Mater.* **2015**, *27*, 5261−5270.

(11) Liu, K.-K.; Tadepalli, S.; Wang, Z.; Jiang, Q.; Singamaneni, S. Structure-dependent SERS activity of plasmonic nanorattles with built-in electromagnetic hotspots. *Analyst* **2017**, *142*, 4536−4543.

(12) Song, X.; Yi, W.; Li, J.; Kong, Q.; Bai, H.; Xi, G. Selective Preparation of Mo2N and MoN with High Surface Area for Flexible SERS Sensing. *Nano Lett.* **2021**, *21*, 4410−4414.

(13) Tanzid, M.; Sobhani, A.; DeSantis, C. J.; Cui, Y.; Hogan, N. J.; Samaniego, A.; Veeraraghavan, A.; Halas, N. J. Imaging through plasmonic nanoparticles. *Proc. Natl. Acad. Sci. U.S.A.* **2016**, *113*, 5558.

(14) Ohannesian, N.; Misbah, I.; Lin, S. H.; Shih, W.-C. Plasmonic nano-aperture label-free imaging (PANORAMA). *Nat. Commun.* **2020**, *11*, No. 5805.

(15) Tian, L.; Gandra, N.; Singamaneni, S. Monitoring Controlled Release of Payload from Gold Nanocages Using Surface Enhanced Raman Scattering. *ACS Nano* **2013**, *7*, 4252−4260.

(16) Dreaden, E. C.; Alkilany, A. M.; Huang, X.; Murphy, C. J.; El-Sayed, M. A. The golden age: gold nanoparticles for biomedicine. *Chem. Soc. Rev.* **2012**, *41*, 2740−2779.

(17) Anker, J. N.; Hall, W. P.; Lyandres, O.; Shah, N. C.; Zhao, J.; Van Duyne, R. P. Biosensing with plasmonic nanosensors. *Nat. Mater.* **2008**, *7*, 442−453.

(18) Liu, K.-K.; Tadepalli, S.; Kumari, G.; Banerjee, P.; Tian, L.; Jain, P. K.; Singamaneni, S. Polarization-Dependent Surface-Enhanced Raman Scattering Activity of Anisotropic Plasmonic Nanorattles. *J. Phys. Chem. C* **2016**, *120*, 16899−16906.

(19) Dang, H.; Park, S.-G.; Wu, Y.; Choi, N.; Yang, J.-Y.; Lee, S.; Joo, S.-W.; Chen, L.; Choo, J. Reproducible and Sensitive Plasmonic Sensing Platforms Based on Au-Nanoparticle-Internalized Nano-dimpled Substrates. *Adv. Funct. Mater.* **2021**, *31*, No. 2105703.

(20) Park, H.-S.; Park, J.; Kwak, J. Y.; Hwang, G.-W.; Jeong, D.-S.; Lee, K.-S. Novel nano-plasmonic sensing platform based on vertical conductive bridge. *Sci. Rep.* **2021**, *11*, No. 3184.

(21) Schlücker, S. Surface-Enhanced Raman Spectroscopy: Concepts and Chemical Applications. *Angew. Chem., Int. Ed.* **2014**, *53*, 4756−4795.

(22) Yu, M.; Huang, Z.; Liu, Z.; Chen, J.; Liu, Y.; Tang, L.; Liu, G. Annealed gold nanoshells with highly-dense hotspots for large-area efficient Raman scattering substrates. *Sens. Actuators, B* **2018**, *262*, 845−851.

(23) Yaghi, O. M.; O'Keeffe, M.; Ockwig, N. W.; Chae, H. K.; Eddaoudi, M.; Kim, J. Reticular synthesis and the design of new materials. *Nature* **2003**, *423*, 705−714.

(24) Furukawa, H.; Cordova Kyle, E.; O'Keeffe, M.; Yaghi Omar, M. The Chemistry and Applications of Metal-Organic Frameworks. *Science* **2013**, *341*, No. 1230444.

(25) Wang, C.; Tadepalli, S.; Luan, J.; Liu, K.-K.; Morrissey, J. J.; Kharasch, E. D.; Naik, R. R.; Singamaneni, S. Metal-Organic Framework as a Protective Coating for Biodiagnostic Chips. *Adv. Mater.* **2017**, *29*, No. 1604433.
(26) Ma, L.; Abney, C.; Lin, W. Enantioselective catalysis with homochiral metal−organic frameworks. *Chem. Soc. Rev.* **2009**, *38*, 1248−1256.
(27) Pascanu, V.; González Miera, G.; Inge, A. K.; Martín-Matute, B. Metal−Organic Frameworks as Catalysts for Organic Synthesis: A Critical Perspective. *J. Am. Chem. Soc.* **2019**, *141*, 7223−7234.
(28) Li, B.; Wen, H.-M.; Zhou, W.; Chen, B. Porous Metal−Organic Frameworks for Gas Storage and Separation: What, How, and Why? *J. Phys. Chem. Lett.* **2014**, *5*, 3468−3479.
(29) Ma, S.; Zhou, H.-C. Gas storage in porous metal−organic frameworks for clean energy applications. *Chem. Commun.* **2010**, *46*, 44−53.
(30) Lawson, H. D.; Walton, S. P.; Chan, C. Metal−Organic Frameworks for Drug Delivery: A Design Perspective. *ACS Appl. Mater. Interfaces* **2021**, *13*, 7004−7020.
(31) Sun, H.; Cong, S.; Zheng, Z.; Wang, Z.; Chen, Z.; Zhao, Z. Metal−Organic Frameworks as Surface Enhanced Raman Scattering Substrates with High Tailorability. *J. Am. Chem. Soc.* **2019**, *141*, 870−878.
(32) Ding, Q.; Wang, J.; Chen, X.; Liu, H.; Li, Q.; Wang, Y.; Yang, S. Quantitative and Sensitive SERS Platform with Analyte Enrichment and Filtration Function. *Nano Lett.* **2020**, *20*, 7304−7312.
(33) Yang, X.; Liu, Y.; Lam, S. H.; Wang, J.; Wen, S.; Yam, C.; Shao, L.; Wang, J. Site-Selective Deposition of Metal−Organic Frameworks on Gold Nanobipyramids for Surface-Enhanced Raman Scattering. *Nano Lett.* **2021**, *21*, 8205−8212.
(34) Chen, N.; Xiao, T.-H.; Luo, Z.; Kitahama, Y.; Hiramatsu, K.; Kishimoto, N.; Itoh, T.; Cheng, Z.; Goda, K. Porous carbon nanowire array for surface-enhanced Raman spectroscopy. *Nat. Commun.* **2020**, *11*, No. 4772.
(35) Pan, Y.; Sun, K.; Liu, S.; Cao, X.; Wu, K.; Cheong, W.-C.; Chen, Z.; Wang, Y.; Li, Y.; Liu, Y.; Wang, D.; Peng, Q.; Chen, C.; Li, Y. Core−Shell ZIF-8@ZIF-67-Derived CoP Nanoparticle-Embedded N-Doped Carbon Nanotube Hollow Polyhedron for Efficient Overall Water Splitting. *J. Am. Chem. Soc.* **2018**, *140*, 2610−2618.
(36) Jaiswal, A.; Tian, L.; Tadepalli, S.; Liu, K.-k.; Fei, M.; Farrell, M. E.; Pellegrino, P. M.; Singamaneni, S. Plasmonic Nanorattles with Intrinsic Electromagnetic Hot-Spots for Surface Enhanced Raman Scattering. *Small* **2014**, *10*, 4287−4292.
(37) Xia, X.; Wang, Y.; Ruditskiy, A.; Xia, Y. 25th Anniversary Article: Galvanic Replacement: A Simple and Versatile Route to Hollow Nanostructures with Tunable and Well-Controlled Properties. *Adv. Mater.* **2013**, *25*, 6313−6333.
(38) Ahmad, N.; Bon, M.; Passerone, D.; Erni, R. Template-Assisted in Situ Synthesis of Ag@Au Bimetallic Nanostructures Employing Liquid-Phase Transmission Electron Microscopy. *ACS Nano* **2019**, *13*, 13333−13342.
(39) Shi, Y.; Lyu, Z.; Zhao, M.; Chen, R.; Nguyen, Q. N.; Xia, Y. Noble-Metal Nanocrystals with Controlled Shapes for Catalytic and Electrocatalytic Applications. *Chem. Rev.* **2021**, *121*, 649−735.
(40) Chen, J.; Wiley, B.; McLellan, J.; Xiong, Y.; Li, Z.-Y.; Xia, Y. Optical Properties of Pd−Ag and Pt−Ag Nanoboxes Synthesized via Galvanic Replacement Reactions. *Nano Lett.* **2005**, *5*, 2058−2062.
(41) Huang, X.; Neretina, S.; El-Sayed, M. A. Gold Nanorods: From Synthesis and Properties to Biological and Biomedical Applications. *Adv. Mater.* **2009**, *21*, 4880−4910.
(42) Orendorff, C. J.; Murphy, C. J. Quantitation of Metal Content in the Silver-Assisted Growth of Gold Nanorods. *J. Phys. Chem. B* **2006**, *110*, 3990−3994.
(43) Okuno, Y.; Nishioka, K.; Kiya, A.; Nakashima, N.; Ishibashi, A.; Niidome, Y. Uniform and controllable preparation of Au−Ag core−shell nanorods using anisotropic silver shell formation on gold nanorods. *Nanoscale* **2010**, *2*, 1489−1493.
(44) Jiang, R.; Chen, H.; Shao, L.; Li, Q.; Wang, J. Unraveling the Evolution and Nature of the Plasmons in (Au Core)−(Ag Shell) Nanorods. *Adv. Mater.* **2012**, *24*, OP200−OP207.
(45) Eslava, S.; Zhang, L.; Esconjauregui, S.; Yang, J.; Vanstreels, K.; Baklanov, M. R.; Saiz, E. Metal-Organic Framework ZIF-8 Films As Low-κ Dielectrics in Microelectronics. *Chem. Mater.* **2013**, *25*, 27−33.
(46) Nozari, V.; Calahoo, C.; Tuffnell, J. M.; Keen, D. A.; Bennett, T. D.; Wondraczek, L. Ionic liquid facilitated melting of the metal-organic framework ZIF-8. *Nat. Commun.* **2021**, *12*, No. 5703.
(47) Zheng, F.; Yang, Y.; Chen, Q. High lithium anodic performance of highly nitrogen-doped porous carbon prepared from a metal-organic framework. *Nat. Commun.* **2014**, *5*, No. 5261.
(48) Park, K. S.; Ni, Z.; Côté, A. P.; Choi, J. Y.; Huang, R.; Uribe-Romo, F. J.; Chae, H. K.; O'Keeffe, M.; Yaghi, O. M. Exceptional chemical and thermal stability of zeolitic imidazolate frameworks. *Proc. Natl. Acad. Sci. U.S.A.* **2006**, *103*, 10186.
(49) Panchariya, D. K.; Rai, R. K.; Anil Kumar, E.; Singh, S. K. Core−Shell Zeolitic Imidazolate Frameworks for Enhanced Hydrogen Storage. *ACS Omega* **2018**, *3*, 167−175.
(50) Li, S.; Zhang, X.; Huang, Y. Zeolitic imidazolate framework-8 derived nanoporous carbon as an effective and recyclable adsorbent for removal of ciprofloxacin antibiotics from water. *J. Hazard. Mater.* **2017**, *321*, 711−719.
(51) Luanwuthi, S.; Krittayavathananon, A.; Srimuk, P.; Sawangphruk, M. In situ synthesis of permselective zeolitic imidazolate framework-8/graphene oxide composites: rotating disk electrode and Langmuir adsorption isotherm. *RSC Adv.* **2015**, *5*, 46617−46623.
(52) Zhang, Y.; Jia, Y.; Li, M.; Hou, L. A. Influence of the 2-methylimidazole/zinc nitrate hexahydrate molar ratio on the synthesis of zeolitic imidazolate framework-8 crystals at room temperature. *Sci. Rep.* **2018**, *8*, No. 9597.
(53) Guo, H.; Yin, Z.; Namkoong, M.; Li, Y.; Nguyen, T.; Salcedo, E.; Arizpe, I.; Tian, L. Printed Ultrastable Bioplasmonic Microarrays for Point-of-Need Biosensing. *ACS Appl. Mater. Interfaces* **2022**, *14*, 10729−10737.
(54) Zheng, G.; de Marchi, S.; López-Puente, V.; Sentosun, K.; Polavarapu, L.; Pérez-Juste, I.; Hill, E. H.; Bals, S.; Liz-Marzán, L. M.; Pastoriza-Santos, I.; Pérez-Juste, J. Encapsulation of Single Plasmonic Nanoparticles within ZIF-8 and SERS Analysis of the MOF Flexibility. *Small* **2016**, *12*, 3935−3943.

https://doi.org/10.1021/acsomega.2c04183
ACS Omega 2022, 7, 36427−36433